



## Quasi 3D Refined Simulation of Flow and Pollutant Transport in The Mississippi River near The Rock Lake

Li-ren Yu<sup>1,2</sup>

1.ESDV (Environmental Software and Digital Visualization), Rm.302, Unit4, Building420, Wan-Sheng-Bei-Li, Ton-Zhou Dist., 101121, Beijing, China.

2.ASSER-CESUSC (Association of United Schools-Higher Education Center at São Carlos), Brazil

### Abstract

This paper reports a quasi 3D numerical simulation in a curved river reach of the Mississippi River near The Rock Lake, USA, aiming to develop a numerical tool for modeling turbulent flows and pollutant transport in complex natural waters. The recently built depth-averaged two-equation turbulence  $\tilde{k} - \tilde{\omega}$  model, together with  $\tilde{k} - \tilde{\epsilon}$  and  $\tilde{k} - \tilde{w}$  models, were used to close non-simplified quasi 3D hydrodynamic fundamental governing equations. The discretized equations were solved by advanced multi-grid iterative method under non-orthogonal body-fitted coarse and fine two-levels' grids with collocated variable arrangement. Except for steady flow and transport computation, the processes of contaminant inpouring and plume development, caused by the side-discharge from a tributary, also have been investigated numerically. The used three closure approaches are suitable for modeling strong mixing turbulence. The established  $\tilde{k} - \tilde{\omega}$  model with higher order of magnitude of transported variable  $\tilde{\omega}$  provides a possibility to elevate the computational precision. Based on the developed hydrodynamic model, a CFD (*Computational Fluid Dynamics*) software, namely **Q3drm1.0**, was developed. This tool focuses on the refined simulations of the steady and unsteady problems of flow and temperature/contaminant transports in complicated computational domains with a strong ability to deal with different types of discharges: side-discharge, point-source/point-sink, and area-source discharge from the slope along bank. In this paper, only the study of side-discharge is presented.

**Key words:** depth-averaged turbulence models; contaminant transport; river modeling; numerical modeling; multi-grid iterative method

### 1 Introduction

Almost all flows in natural rivers are turbulence. Dealing with the problems of turbulence tightly related to stream pollutions is challenging for scientists and engineers, because of their damaging effect on our fragile environment and limited water resources. It is important to develop adequate mathematical models, turbulence closure models, numerical methods and corresponding analytical tools for timely simulating and predicting contaminant transport behaviors in natural and artificial waters.

Although the significance of modeling turbulent flows and contaminant transport phenomena with a high precision is clear, the numerical simulation and prediction for natural waters with complex geometry and variable bottom topography are still unsatisfied. This is mainly due to the inherent complexity of the problems being considered. Any computation and simulation of flow and transport processes critically depends on following four elements: to generate a suitable computational domain with the ability to deal with non-regular geometrical boundaries, such as curved riversides and island boundaries; to establish practical turbulence closure models with minor numerical error and higher precision; to adopt efficient computational method and algorithm, and to develop corresponding numerical tool, respectively.

Numerous environmental flows can be considered as shallow, *i.e.*, the horizontal length scales of the flow domain are much larger than the depth. Typical examples are found in lowland rivers, lakes, coastal areas, oceanic and stratified atmospheric flows. Depth-averaged mathematical models are frequently used for modelling the flow and contaminant transport in well-mixed shallow waters. However, many models used in practice merely consider the depth-averaged turbulent viscosity and diffusivity through constants or simple phenomenological algebraic formulas (Choi and Takashi 2000; Lunis et al. 2004; Vasquez 2005; Kwan 2009; Viparelli 2010), which are estimated to a great degree according to the modellers' experience. Although some practical quasi 3D hydrodynamic models are really closed by depth-averaged two-equation closure turbulence model, they almost all concentrate on the investigations and applications of classical depth-averaged  $\tilde{k} - \tilde{\epsilon}$  model (Rodi et al. 1980; Chapman and Kuo 1982; Mei et al. 2002; Johnson et al. 2005; Cea et al. 2007; Hua et al. 2008; Kimura et al. 2009; Lee et al. 2011), which appeared already beyond 30 years. It is well known that the order of magnitude of transported variable  $\tilde{\epsilon}$  of  $\tilde{k} - \tilde{\epsilon}$  model is very low indeed.

Recent development of turbulence modeling theory has provided more advanced and realistic closure models. From an engineering perspective, two-equation closure turbulence models can build a higher standard for numerically approximation of main flow behaviors and transport phenomena in terms of efficiency, extensibility and robustness (Yu, 2013). Unfortunately, the 'standard' two-equation closure models, used widely in industry, cannot be directly employed in quasi 3D modeling. The depth-averaged turbulence model, based on the 'standard' two-equation closure model, needs to be established and investigated in advance.

Except for the depth-averaged  $\tilde{k} - \tilde{\omega}$  model closure, newly established by the author, current simulations still adopt the closure approaches of classical depth-averaged  $\tilde{k} - \tilde{\epsilon}$  model and depth-averaged  $\tilde{k} - \tilde{\omega}$  model, respectively. The depth-averaged  $\tilde{k} - \tilde{\omega}$  model was stemmed from the most common 'standard'  $k-\omega$  model, originally introduced by Saffman (1970) but popularized by Wilcox (1998). In this paper, the results, computed by the three depth-averaged two-equation turbulence models, were compared each other. Such example, however, hardly exists for the simulation of contaminant transport in natural waters. Modeling by using different two-equation closure approaches will certainly increase the credibility of users' simulation results (Yu, 2013).

On the other hand, recent advancements in grid generation techniques, numerical methods and IT techniques have provided suitable approaches to generate non-orthogonal boundary-fitted coordinates with collocated grid arrangement, on which the non-simplified hydrodynamic fundamental governing equations can be solved by multi-grid iterative method (Ferziger and Peric 2002). This paper describes a quasi 3D hydrodynamic simulation of flow and contaminant transport in a curved river reach of the Mississippi River, with the aim to develop the *grid-generator*, *flow-solver* and GUI (*Graphical User Interface*). The developed software, named **Q3drm1.0**, provides three selectable depth-averaged two-equation closure turbulence models, and can refinedly solve quasi 3D flow and contaminant transport phenomena in complex natural and artificial waters.

## 2 Hydrodynamic Fundamental Governing Equations

The complete, non-simplified fundamental governing equations of quasi 3D computation, in terms of coordinate-free vector forms derived by using vertical Leibniz integration for a Control Volume (CV, an arbitrary quadrilateral with center point  $P$ ), considering the variation of the bottom topography and water surface and neglecting minor terms in the depth-averaging procedure, can be written as follows:

$$\frac{\partial}{\partial t} \int_{\Omega} \rho h \bar{\phi} d\Omega + \int_S \rho h \bar{\phi} \bar{\mathbf{v}} \cdot \bar{\mathbf{n}} dS = \int_S \Gamma h \mathbf{grad} \bar{\phi} \cdot \bar{\mathbf{n}} dS + \int_{\Omega} \bar{q}_{\phi} d\Omega \quad (1)$$

where  $\Omega$  is the CV's volume;  $S$  is the face;  $\bar{\mathbf{v}}$  is the depth-averaged velocity vector; the superscript “-” indicates that the value is strictly depth-averaged;  $\bar{\phi}$  is any depth-averaged conserved intensive property (for mass

conservation,  $\bar{\phi}=1$ ; for momentum conservation,  $\bar{\phi}$  is the components in different directions of  $\bar{v}$ ; for conservation of a scalar,  $\bar{\phi}$  is the conserved property per unit mass);  $\Gamma$  is the diffusivity for the quantity  $\bar{\phi}$ ;  $\bar{q}_\phi$  denotes the source or sink of  $\bar{\phi}$ ; and  $h$  and  $\rho$  are local water depth at  $P$  and density, respectively.

For the momentum conservation of Eq. (1),  $\Gamma = \tilde{\mu}_{eff}$  (depth-averaged effective viscosity); for temperature or concentration transport,  $\Gamma = \tilde{\Gamma}_{\phi,t}$  (temperature or concentration diffusivity), where the superscript “~” indicates the quantity characterizing depth-averaged turbulence. The source (sink) term  $\bar{q}_\phi$  for momentum conservation may include surface wind shear stresses, bottom shear stresses, pressure terms and additional point sources (or point sinks).

### 3 Depth-Averaged Turbulence Closure Models

The depth-averaged effective viscosity  $\tilde{\mu}_{eff}$  and diffusivity  $\tilde{\Gamma}_{\phi,t}$ , appeared in Eq. (1), are dependent on the molecular dynamic viscosity  $\mu$  and depth-averaged eddy viscosity  $\tilde{\mu}_t$ :  $\tilde{\mu}_{eff} = \mu + \tilde{\mu}_t$  and  $\tilde{\Gamma}_{\phi,t} = \tilde{\mu}_t / \sigma_{\phi,t}$ , where  $\sigma_{\phi,t}$  is the turbulence Prandtl number for temperature diffusion or Schmidt number for concentration diffusion, and  $\tilde{\mu}_t$  is a scalar property and normally determined by two extra transported variables.

Recently, the author established a new depth-averaged two-equation closure turbulence model,  $\tilde{k} - \tilde{\omega}$ , based on the ‘standard’  $k - \omega$  model (in which  $\omega$  is the special dissipation rate), originally introduced by Saffman (1970) but popularized by Wilcox (1998). The ‘standard’  $k - \omega$  turbulence model has been used in engineering researches (Riasi et al. 2009; Kirkgoz et al. 2009). In depth-averaged  $\tilde{k} - \tilde{\omega}$  model, the turbulent viscosity is expressed by:

$$\tilde{\mu}_t = \rho \tilde{k} / \tilde{\omega} \quad (2)$$

where  $\tilde{k}$  and  $\tilde{\omega}$  stand for the depth-averaged turbulent kinetic energy and special dissipation rate of turbulence kinetic energy in the depth-averaged sense. They are determined by solving two extra transport equations, *i.e.*, the  $\tilde{k}$ -eq. and  $\tilde{\omega}$ -eq, respectively. (Yu and Yu, 2009):

$$\frac{\partial(\rho h \tilde{k})}{\partial t} + \text{div}(\rho h \tilde{k} \bar{v}) = \text{div}(h(\mu + \frac{\tilde{\mu}_t}{\sigma_k^*}) \mathbf{grad} \tilde{k}) + h P_k - \rho \beta^* h \tilde{k} \tilde{\omega} + \rho h P_{kv} + \bar{S}_k \quad (3)$$

$$\frac{\partial(\rho h \tilde{\omega})}{\partial t} + \text{div}(\rho h \tilde{\omega} \bar{v}) = \text{div}(h(\mu + \frac{\tilde{\mu}_t}{\sigma_\omega^*}) \mathbf{grad} \tilde{\omega}) + \alpha h \frac{\tilde{\omega}}{\tilde{k}} P_k - \rho h \beta \tilde{\omega}^2 + \rho h P_{\omega} + \bar{S}_\omega \quad (4)$$

where  $\bar{S}_k$  and  $\bar{S}_\omega$  are the source-sink terms,  $P_k = \tilde{\mu}_t \left[ 2 \left( \frac{\partial \bar{u}}{\partial x} \right)^2 + 2 \left( \frac{\partial \bar{v}}{\partial y} \right) + \left( \frac{\partial \bar{u}}{\partial y} + \frac{\partial \bar{v}}{\partial x} \right)^2 \right]$  is the production of

turbulent kinetic energy due to the interactions of turbulent stresses with horizontal mean velocity gradients. The values of empirical constants  $\alpha$ ,  $\beta$ ,  $\beta^*$ ,  $\sigma_k^*$ , and  $\sigma_\omega^*$  in Eq. (3) through Eq. (4) are the same as in the ‘standard’  $k - \omega$  model: 5/9, 0.075, 0.9, 2, and 2. According to the dimensional analysis, the additional source terms  $P_{kv}$  in  $k$ -eq. (3) and  $P_\omega$  in  $\omega$ -eq. (4) are mainly produced by the vertical velocity gradients near the bottom, and can be expressed as follows:

$$P_{kv} = C_k u_*^3 / h, P_\omega = C_\omega u_*^2 / h^2 \quad (5)$$

while the local friction velocity  $u_*$  is equal to  $\sqrt{C_f(\bar{u}^2 + \bar{v}^2)}$ , the empirical constant  $C_\omega$  for open channel flow and rivers can be expressed as:

$$C_\omega = \beta / (C_\mu \times e^* \times C_f^{1/2}) \tag{6}$$

where  $C_f$  represents an empirical friction factor and  $e^*$  is the dimensionless diffusivity of the empirical formula for undisturbed channel/river flows  $\tilde{\mu}_t = e^* U_* h$  with  $U_*$  being the global friction velocity.

Except for the newly developed  $\tilde{k} - \tilde{\omega}$  turbulence model mentioned above, the author also uses depth-averaged  $\tilde{k} - \tilde{\varepsilon}$  model and  $\tilde{k} - \tilde{w}$  model, to close the fundamental governing equations in the current computations. The  $\tilde{k} - \tilde{\varepsilon}$  model was suggested by McGuirk and Rodi as early as in 1977:

$$\frac{\partial(\rho h \tilde{k})}{\partial t} + \text{div}(\rho h \tilde{k} \bar{v}) = \text{div}(h(\mu + \frac{\tilde{\mu}_t}{\sigma_k}) \mathbf{grad} \tilde{k}) + h P_k - \rho h \tilde{\varepsilon} + \rho h P_{kv} + \bar{S}_k \tag{7}$$

$$\frac{\partial(\rho h \tilde{\varepsilon})}{\partial t} + \text{div}(\rho h \tilde{\varepsilon} \bar{v}) = \text{div}(h(\mu + \frac{\tilde{\mu}_t}{\sigma_\varepsilon}) \mathbf{grad} \tilde{\varepsilon}) + C_1 h P_k \frac{\tilde{\varepsilon}}{\tilde{k}} - C_2 \rho h \frac{\tilde{\varepsilon}^2}{\tilde{k}} + \rho h P_{\varepsilon v} + \bar{S}_\varepsilon \tag{8}$$

where  $\bar{S}_k$  and  $\bar{S}_\varepsilon$  are the source-sink terms,  $\tilde{\mu}_t$  can be expressed as:

$$\tilde{\mu}_t = \rho C_\mu \tilde{k}^2 / \tilde{\varepsilon} \tag{9}$$

where  $\tilde{\varepsilon}$  stands for dissipation rate of  $\tilde{k}$ . The values of empirical constants  $C_\mu$ ,  $\sigma_k$ ,  $\sigma_\varepsilon$ ,  $C_1$  and  $C_2$  in Eqs. (7-9) are the same as the 'standard'  $k-\varepsilon$  model, i.e. equal to 0.09, 1.0, 1.3, 1.44 and 1.92, respectively. The additional source terms  $P_{kv}$  and  $P_{\varepsilon v}$  in Eqs. (7) and (8) can be written by:

$$P_{kv} = C_k u_*^3 / h, P_{\varepsilon v} = C_\varepsilon u_*^4 / h^2 \tag{10}$$

where the empirical constants  $C_k$  and  $C_\varepsilon$  for open channel flow and rivers are:

$$C_k = 1 / \sqrt{C_f}, C_\varepsilon = C_2 C_\mu^{1/2} / (C_f^{3/4} \times e^{*1/2}) \tag{11}$$

The third used depth-averaged second-order closure  $\tilde{k} - \tilde{w}$  model was previously developed by the author of the present paper and his colleague (Yu and Zhang 1989). This model originated from the revised  $k-w$  model developed by Ilegbusi and Spalding (1982). The two extra transport equations of this model (i.e., the  $\tilde{k}$ -eq. and the  $\tilde{w}$ -eq.) should be:

$$\frac{\partial(\rho h \tilde{k})}{\partial t} + \text{div}(\rho h \tilde{k} \bar{v}) = \text{div}(h(\mu + \frac{\tilde{\mu}_t}{\sigma_k}) \mathbf{grad} \tilde{k}) + h P_k + \rho h P_{kv} - C_\mu \rho h \tilde{k} \tilde{w}^{1/2} + \bar{S}_k \tag{12}$$

$$\begin{aligned} \frac{\partial(\rho h \tilde{w})}{\partial t} + \text{div}(\rho h \tilde{w} \bar{v}) = & \text{div}(h(\mu + \frac{\tilde{\mu}_t}{\sigma_\varepsilon}) \mathbf{grad} \tilde{w}) + C_{1w} \tilde{\mu}_t h (\mathbf{grad} \Omega)^2 \\ & - C_{2w} \rho h \tilde{w}^{3/2} f + C_{3w} h \frac{\tilde{w}}{\tilde{k}} P_k + \rho h P_{wv} + \bar{S}_w \end{aligned} \tag{13}$$

where  $\bar{S}_k$  and  $\bar{S}_w$  are the source-sink terms; function  $f = 1 + C'_{2w} (\partial L / \partial x_i)$  and  $L$  is the characteristic distance of turbulence;  $\Omega$  stands for mean movement vorticity. In  $\tilde{k} - \tilde{w}$  model, the turbulent viscosity is defined as:

$$\tilde{\mu}_t = \rho \tilde{k} / \tilde{w}^{1/2} \tag{14}$$

where  $\tilde{w}$  is depth-averaged time-mean-square vorticity fluctuation of turbulence. The transport equations (the  $\tilde{k}$ -eq. and  $\tilde{w}$ -eq.) should be solved in this model as well. The values of empirical constants  $C_\mu$ ,  $\sigma_k$ ,  $\sigma_w$ ,  $C_{1w}$ ,  $C_{2w}$ ,  $C'_{2w}$  and  $C_{3w}$  are the same as those of 'standard'  $k-w$  model, i.e., equal 0.09, 1.0, 1.0, 3.5, 0.17, 17.47 and

1.12, respectively. The corresponding additional source terms  $P_{kv}$  and  $P_{wv}$ , also mainly due to the vertical velocity gradients near the bottom, and can be expressed as:

$$P_{kv} = C_k u_*^3 / h, P_{wv} = C_w u_*^3 / h^3 \quad (15)$$

The empirical constants  $C_w$  for open channel flow and rivers can be written as:

$$C_w = C_{2w} / (C_\mu^{3/2} \times C_f^{3/4} \times e^{*3/2}) \quad (16)$$

The mathematical model and turbulence models, developed by the author, have been numerically investigated with laboratorial and site data for different flow situations (Yu and Zhang 1989; Yu and Righetto 2001). In the established mathematical model, the original empirical constants of three depth-averaged turbulence models, suggested by their authors, are employed and do not been changed never.

Figure 1 displays a comparison between the fine light-blue concentration contour with  $35\text{mg/L}$ , calculated by using  $\tilde{k} - \tilde{\omega}$  model closure on fine grid and plotted by the field browser of **Q3drm1.0**, and the outline of black-water plume, shown on the *Google* satellite map. In this computation, one reach of the Amazon River, near the Manaus City, Brazil, has been computed, where the Negro River flows into the Solimões River from the North and West to form the Amazon River below this city. The confluent tributaries, in the Amazon's water system, usually have concentration difference in comparison with the mainstream, caused by the humus in tropical rain forest (produced by tropic rains). The Negro River, however, is the largest left tributary of the Amazon and the largest black-water river in the world. In this figure, the coarse yellow lines demonstrate the outline of computational domain. It is clear that the simulated depth-averaged contour, however, is well coincident with the outline of black-water plume.

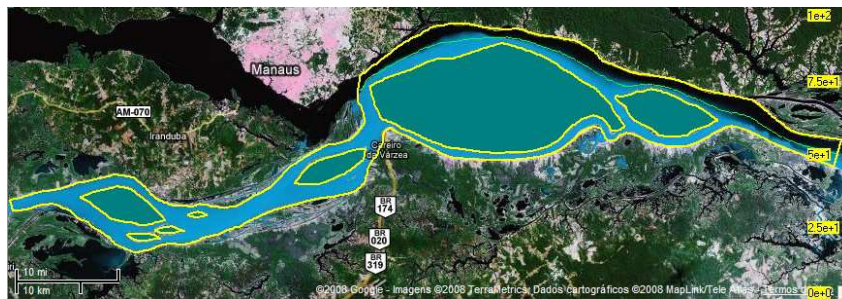


Fig. 1 Comparison between calculated concentration contour and black-water plume outline.

#### 4 Grid Generation

In this paper, one reach of the Mississippi River near the Rock Lake, has been computed by using the *grid-generator* and *flow-solver*, written in FORTRAN Language, where a small tributary flows into this river from his left bank. The confluent tributary has a concentration difference in comparison with the mainstream. With the help of the developed software, it is possible to determine the scale of digital map (*Google Earth*), to collect conveniently geometrical data, including the positions of two curved riversides, two boundaries of one island and the location of confluent tributary section, and finally to generate one text file. In this file, all of messages, which illustrate necessary control variables and characteristic parameters, including those on four exterior boundaries (north inlet section, south outlet section, west and east riversides) are contained, and can be read by *grid-generator* to generate the expectant coarse and fine grids (two levels' grids).

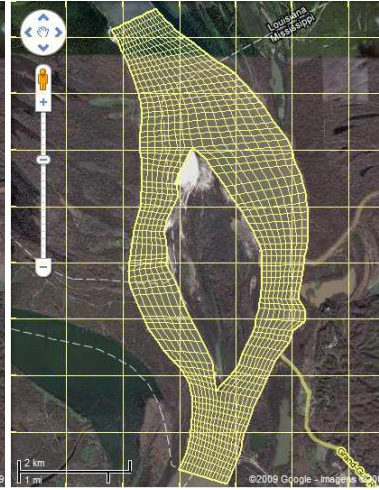
Fig. 2 Map, plotted by *interface*.

Fig. 3 Coarse grid.

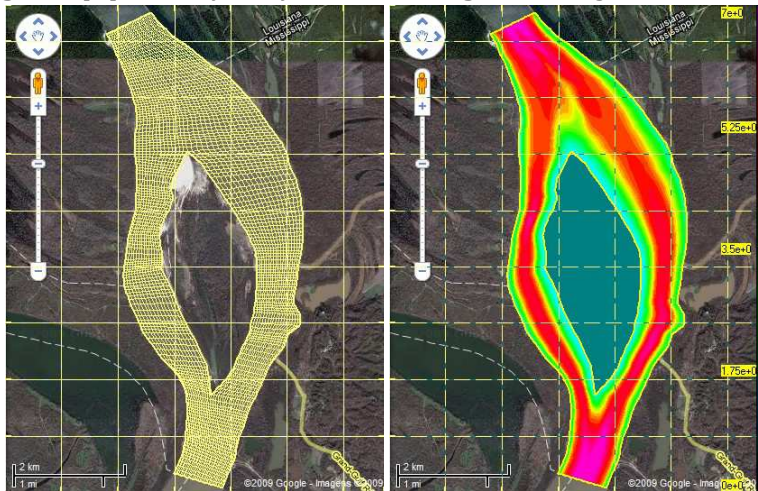


Fig. 4 Fine grid.

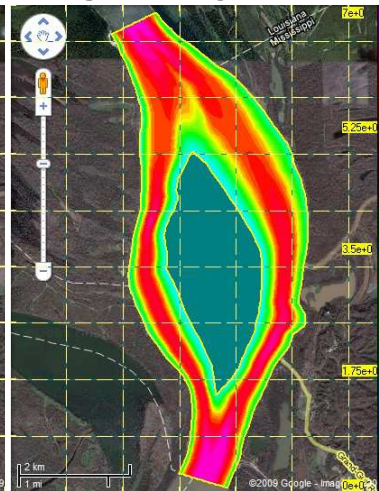


Fig. 5 Bottom topography.

Figure 2 demonstrates the digital map, on which the developed *interface* of **Q3drm1.0** has divided the computational river reach into 35 sub-reaches with 36 short cross-river lines (*i.e.*,  $NLRs=36$ ). It is notable that the cross-river lines between the riverside and island boundary have been redrawn, in order to involve the island configuration. Figure 3 presents the generated body-fitted non-orthogonal coarse grid, drawn by the grid-browser of **Q3drm1.0**, with the resolution of 18 nodal points in  $i$ -direction and 71 nodal points in  $j$ -direction, respectively. In this example, the  $i$ -direction is from the West to the East (*i.e.*  $IDIR=1$ ). In the generated mesh, the nodal points on transversal grid lines are uniform. The total length of the calculated river reach is 9.1km. The flow direction is from the North to the South. The tributary feeds into the mainstream on the west riverside, with the numbers of nodal points from  $j=33$  on the coarse computational grid. The one islands start at  $(i=8, j=14)$  and ends at  $(i=8, j=48)$  on the same mesh. The developed *grid-generator* generated two layers' grids, on which all of geometric data, necessary in the later calculation of flow and contaminant transport, must be stored and then can be read by the developed *flow-solver*. The resolution of the fine grid is  $34 \times 140$ , displayed on Figure 4. This means that one volume cell on the coarse grid was divided into four volume cells on the fine grid. Figure 5 represents the bottom topography on fine grid, drawn by the field browser of **Q3drm1.0**. During the calculation, the variation of bottom topography was considered. On Figures 3-5, the interval between two horizontal and vertical coordinate lines is 1km.

### 5 Solutions of Flow and Side Discharge

The behaviors of flows and transport were simulated by using the developed *flow-solver*, in which the SIMPLE (*Semi-Implicit Method for Pressure-Linked Equation*) algorithm for FVA (*Finite Volume Approach*), Gauss' divergence theorem, ILU (*Incomplete Lower-Upper*) decomposition, PWIM (*Pressure Weighting Interpolation Method*), SIP (*Strongly Implicit Procedure*), under relaxation and multi-grid iterative method have been used. The

hydrodynamic fundamental governing equations were solved firstly at the coarse grid and then at the fine grid, in the following sequence for each grid level: two momentum equations ( $\bar{u}$ -eq. and  $\bar{v}$ -eq.), one pressure-correction equation ( $p'$ -eq.), one concentration transport equation ( $\bar{C}_1$ -eq.), and two transport equations (*i.e.*, the  $\tilde{k}$ -eq. and  $\tilde{\epsilon}$ -eq.; or  $\tilde{k}$ -eq. and  $\tilde{w}$ -eq.; or  $\tilde{k}$ -eq. and  $\tilde{\omega}$ -eq.), respectively.

The calculated main stream flow-rate is  $9,000\text{m}^3/\text{s}$ , while the width, area and mean water-depth of the inlet section are  $872.99\text{m}$ ,  $5,074\text{m}^2$  e  $5.813\text{m}$ . The empirical friction factor ( $C_f$ ) equals 0.00273. The flow-rate and concentration difference of tributary are  $200\text{m}^3/\text{s}$  and  $100\text{mg}/\text{L}$ , respectively. Three depth-averaged two-equation closure turbulence models, *i.e.*, the  $\tilde{k} - \tilde{\epsilon}$ ,  $\tilde{k} - \tilde{w}$  and  $\tilde{k} - \tilde{\omega}$  models, are adopted to close the quasi 3D hydrodynamic model. The turbulent variables at the inlet sections can be calculated by empirical formulae, *i.e.*,  $\tilde{k}_0$ ,  $\tilde{\epsilon}_0$ ,  $\tilde{w}_0$ ,  $\tilde{\omega}_0$  are  $0.0966\text{m}^2/\text{s}^2$ ,  $0.0026\text{m}^2/\text{s}^3$ ,  $0.522/\text{s}^2$ ,  $0.2996/\text{s}$ , and  $\tilde{k}_{tri}$ ,  $\tilde{\epsilon}_{tri}$ ,  $\tilde{w}_{tri}$ ,  $\tilde{\omega}_{tri}$  equal  $0.1067\text{m}^2/\text{s}^2$ ,  $0.0061\text{m}^2/\text{s}^3$ ,  $0.806/\text{s}^2$ ,  $0.635/\text{s}$ , respectively. On the outlet section, the variables satisfy constant gradient condition. The wall function approximation was used for determining the values of velocity components and turbulent variables at the nodal points in the vicinity of riversides and island's boundaries.

Due to the existence of two islands in mesh, the values of the under-relaxation factors for velocity components, pressure, concentration and two turbulence parameters are usually lower than those while no exists any island in the mash. Generally, for non-existence of island, they are 0.6, 0.6, 0.1, 0.7, 0.7 and 0.7. In this example, these factors are 0.3, 0.3, 0.05, 0.7, 0.35 and 0.35, respectively. The maximum allowed numbers of inner iteration for solving velocity components, pressure, concentration and two turbulent variables are 1, 1, 20, 1, 1 and 1. The convergence criterions for inner iteration are 0.1, 0.1, 0.01, 0.1, 0.01 and 0.01, respectively. The  $\alpha$  parameter of the Stone's solver is equal to 0.92. The normalize residuals for solving velocity field, pressure field, concentration field and the fields of two transported variables of turbulence are all less than pre-determined convergence criterion ( $1.e-3$ ).

The simulation obtained various 2D and 3D distributions of flow, pressure, concentration and turbulent variables and parameters, which are useful to analyze interested problems in engineering. **Q3drm1.0** provides powerful profile browser, field browser and 3D browser for plotting and analyzing computational results. A part of results, simulated by using  $\tilde{k} - \tilde{\epsilon}$ ,  $\tilde{k} - \tilde{w}$  and  $\tilde{k} - \tilde{\omega}$  models on the fine grid, are presented from Figure 6 to Figure 10. Figure 6 display the results, calculated by using  $\tilde{k} - \tilde{\omega}$  closure model and drawn by the field browser, with a: flow pattern, b: color filled flow field, c: color filled pressure field, d: color concentration contours, e: color filled  $\tilde{k}$  distribution and f: color filled  $\tilde{\omega}$  distribution, respectively. Figure 6d illustrates that the contaminant plume well develops along the left riverside at the lower reach of the tributary outlet section. The distributions of the same depth-averaged physical variables and turbulent variable  $\tilde{k}$ , calculated by  $\tilde{k} - \tilde{\epsilon}$  and  $\tilde{k} - \tilde{w}$  turbulence models, are similar to Figures 6a-6e, except for the distributions of second transported variables (see Figures a-c and Figures a-b). Figures 7a, 7b and 7c demonstrate the 3D distributions of  $\tilde{k}$ , calculated by using these three depth-averaged turbulence models and drawn by the 3D browser. They are quite similar each other, with the maximum values:  $0.5779\text{m}^2/\text{s}^2$  for  $\tilde{k} - \tilde{\omega}$  modeling (7a),  $0.5688\text{m}^2/\text{s}^2$  for  $\tilde{k} - \tilde{\epsilon}$  modeling (7b) and  $0.5684\text{m}^2/\text{s}^2$  for  $\tilde{k} - \tilde{w}$  modeling (7c), respectively. Figures 8a, 8b and 8c present the 3D distributions of  $\tilde{\omega}$ ,  $\tilde{\epsilon}$  and  $\tilde{w}$ , which are different each other, because of the different definitions of the used second transported variables in current computations. Actually, the  $\tilde{\epsilon}$  value, shown in Figure 8b, ranges only from  $5.588e-6$  to  $1.11e-2\text{m}^2/\text{s}^3$ ; however, the  $\tilde{w}$  and  $\tilde{\omega}$  range from  $1.342e-4$  to  $1.012/\text{s}^2$  and from  $1.132e-2$  to  $0.997/\text{s}$  in Figure 8c and Figure 8a respectively. Figures 9a, 9b and 9c illustrate the 3D distributions of effective viscosity  $\tilde{\mu}_{eff}$ , while the depth-averaged turbulent eddy viscosity  $\tilde{\mu}_t$  was calculated by using Eq. (2) for  $\tilde{k} - \tilde{\omega}$  modeling (9a), Eq. (9) for  $\tilde{k} - \tilde{\epsilon}$  modeling (9b) and Eq. (14) for  $\tilde{k} - \tilde{w}$  modeling (9c), respectively. Basically, they are similar each other, specially for  $\tilde{k} - \tilde{\epsilon}$  and

$\tilde{k} - \tilde{w}$  modeling, while the maximum values of  $\tilde{\mu}_{eff}$  are 3554.2Pa.s (9b) and 3552.98Pa.s (9c); but the same value for  $\tilde{k} - \tilde{\omega}$  modeling is 3583.16Pa.s (9a). Figure 10 shows the distributions of the production term of turbulent kinetic energy, with the maximum values of  $P_k$  3.811Pa.m/s for  $\tilde{k} - \tilde{\omega}$  modeling (10a), 3.772Pa.m/s for  $\tilde{k} - \tilde{\epsilon}$  modeling (10b) and 3.771Pa.m/s for  $\tilde{k} - \tilde{w}$  modeling (10c). They are also similar each other. Figures 11a and 11b display the comparisons of concentration profiles along the centers of the volume cells at  $i=33$  and  $j$  from 1 to 140 (i.e., along a curved line from the outlet to the inlet near the east riverside) and at  $j=40$  and  $i$  from 1 to 34 (i.e., along a transversal section of  $j=40$ ) on the fine grid, calculated by the depth-averaged  $\tilde{k} - \tilde{\epsilon}$ ,  $\tilde{k} - \tilde{w}$  and  $\tilde{k} - \tilde{\omega}$  turbulence models, respectively. Figure 12a demonstrates the comparisons between  $\tilde{\epsilon}$ ,  $\tilde{w}$  and  $\tilde{\omega}$  along the curved line at  $i=32$ , and Figure 12b the comparisons of these three variables at  $j=40$ 's transversal section, which crosses the island. It is well known that the orders of magnitudes of  $\tilde{\epsilon}$ ,  $\tilde{w}$  and  $\tilde{\omega}$ , used in three turbulence models, have significant differences indeed.

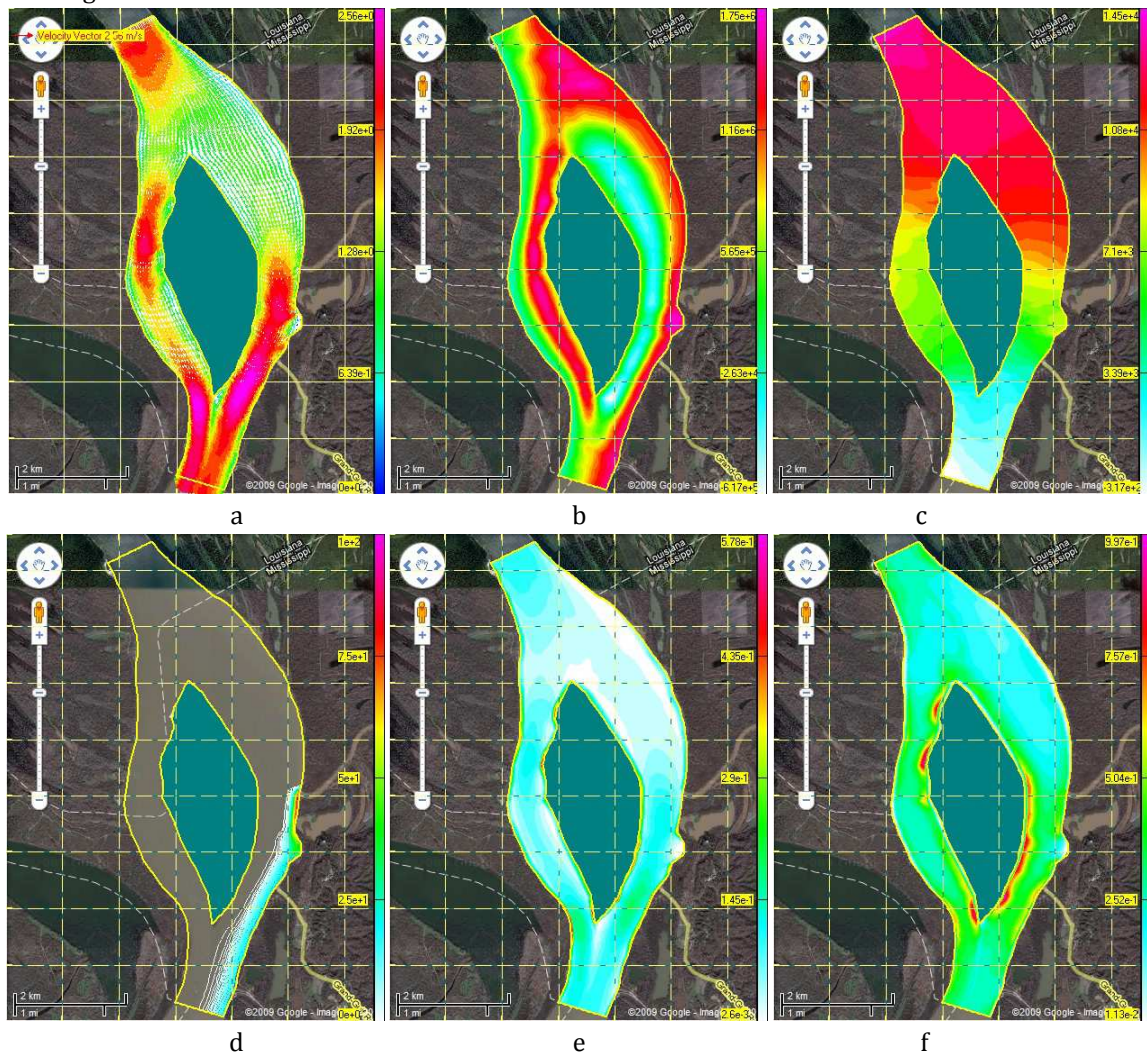


Fig. 6 A part of results, calculated by  $\tilde{k} - \tilde{\omega}$  model.



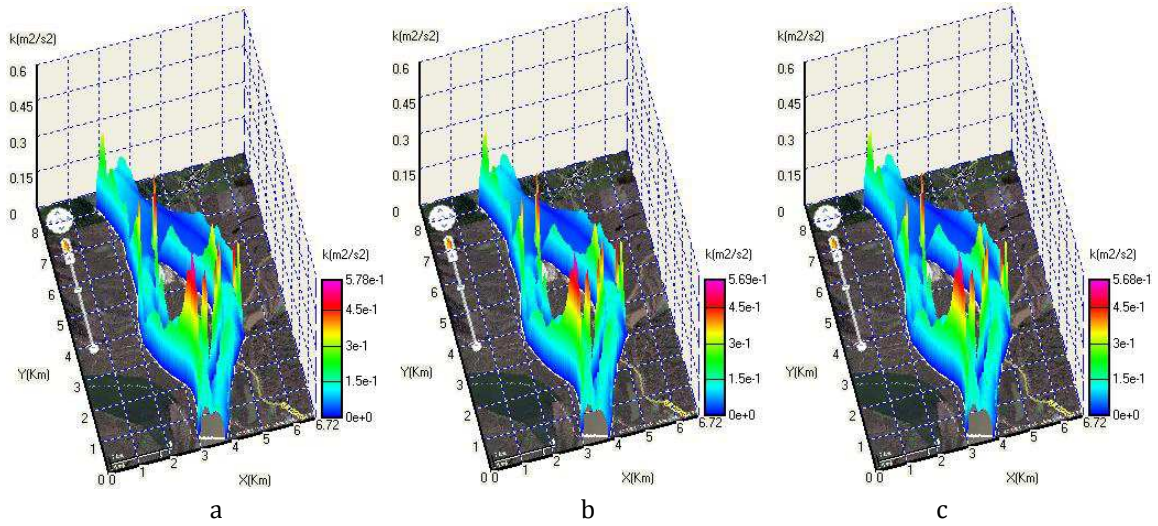


Fig. 7 3D  $\tilde{k}$  distributions, calculated by  $\tilde{k} - \tilde{\omega}$ ,  $\tilde{k} - \tilde{\epsilon}$  and  $\tilde{k} - \tilde{w}$  models.

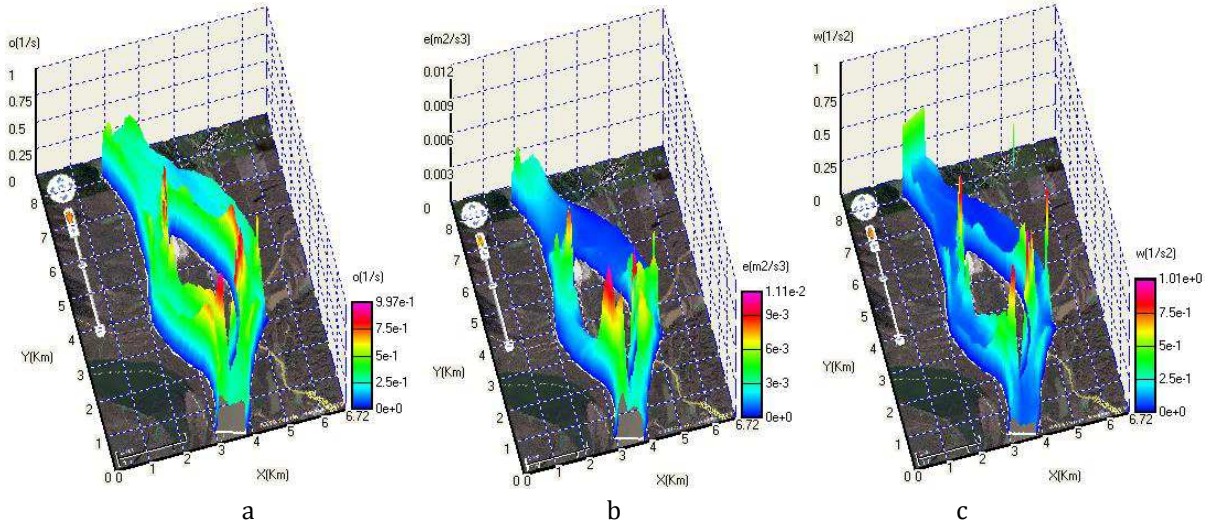


Fig. 8 3D  $\tilde{\omega}$ ,  $\tilde{\epsilon}$  and  $\tilde{w}$  distributions.

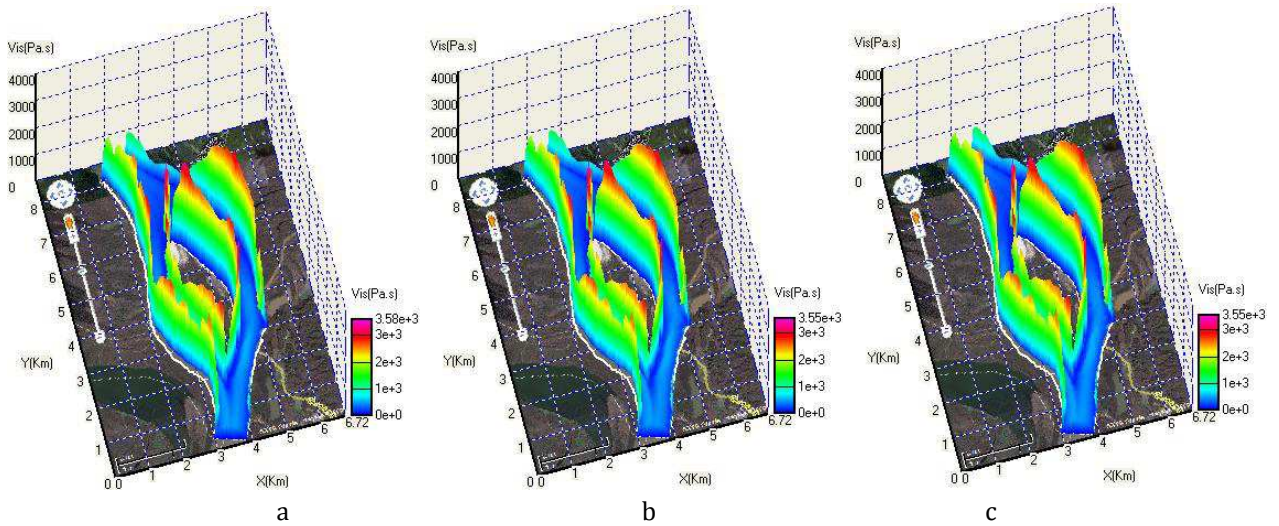


Fig. 9 3D  $\tilde{\mu}_{eff}$  distributions, calculated by  $\tilde{k} - \tilde{\omega}$ ,  $\tilde{k} - \tilde{\epsilon}$  and  $\tilde{k} - \tilde{w}$  models.

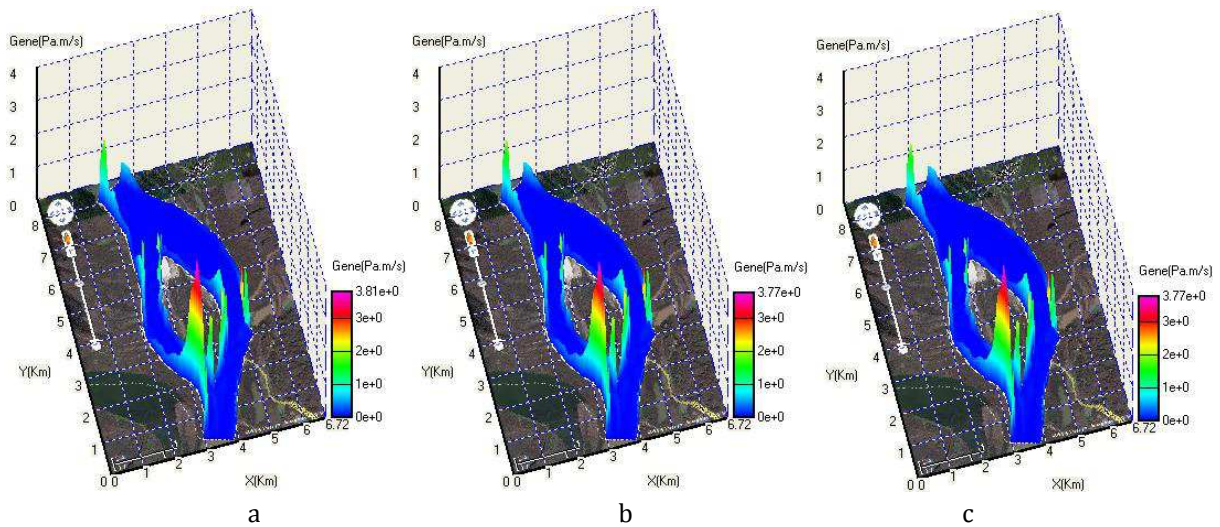


Fig. 10  $P_k$  distributions, calculated by  $\tilde{k} - \tilde{\omega}$ ,  $\tilde{k} - \tilde{\epsilon}$  and  $\tilde{k} - \tilde{w}$  models

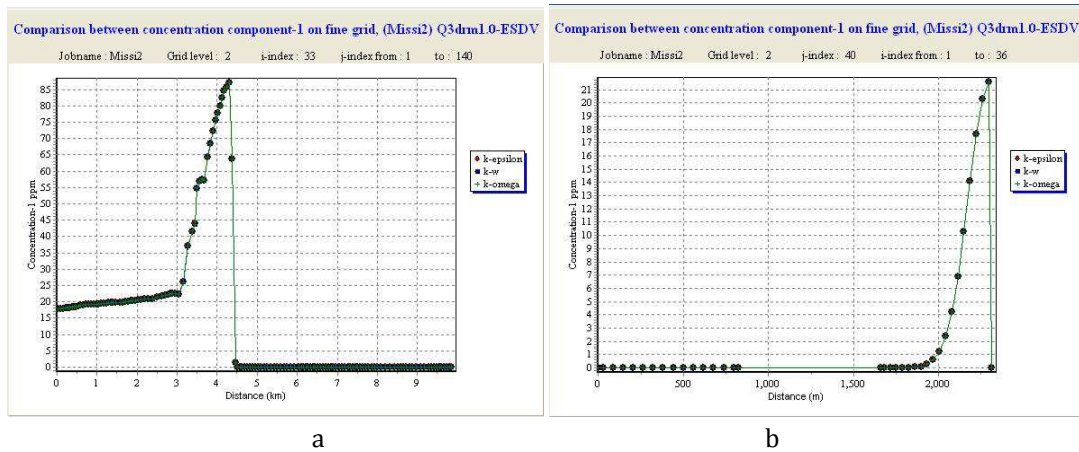


Fig. 11 Concentrations at a:  $i=33$  and  $j$  from 1 to 140; b:  $i$  from 1 to 34 and  $j=40$ .

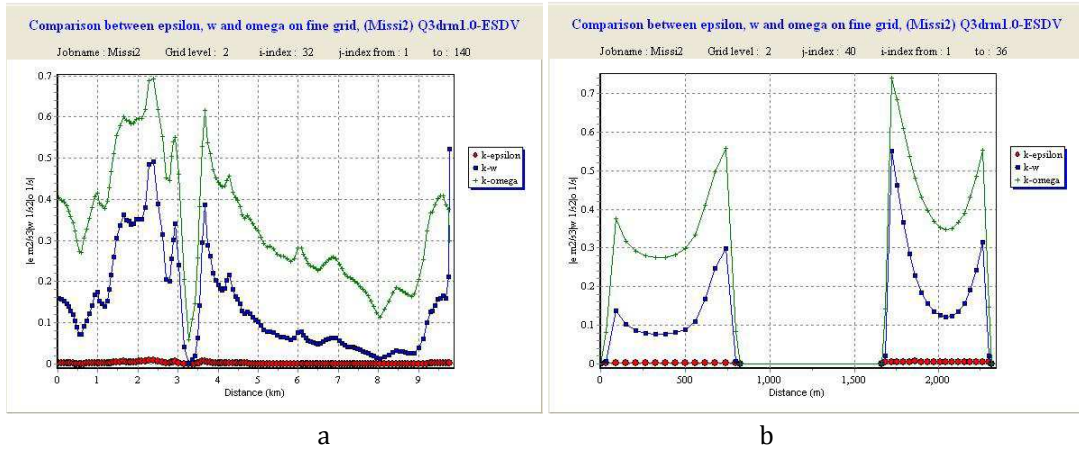
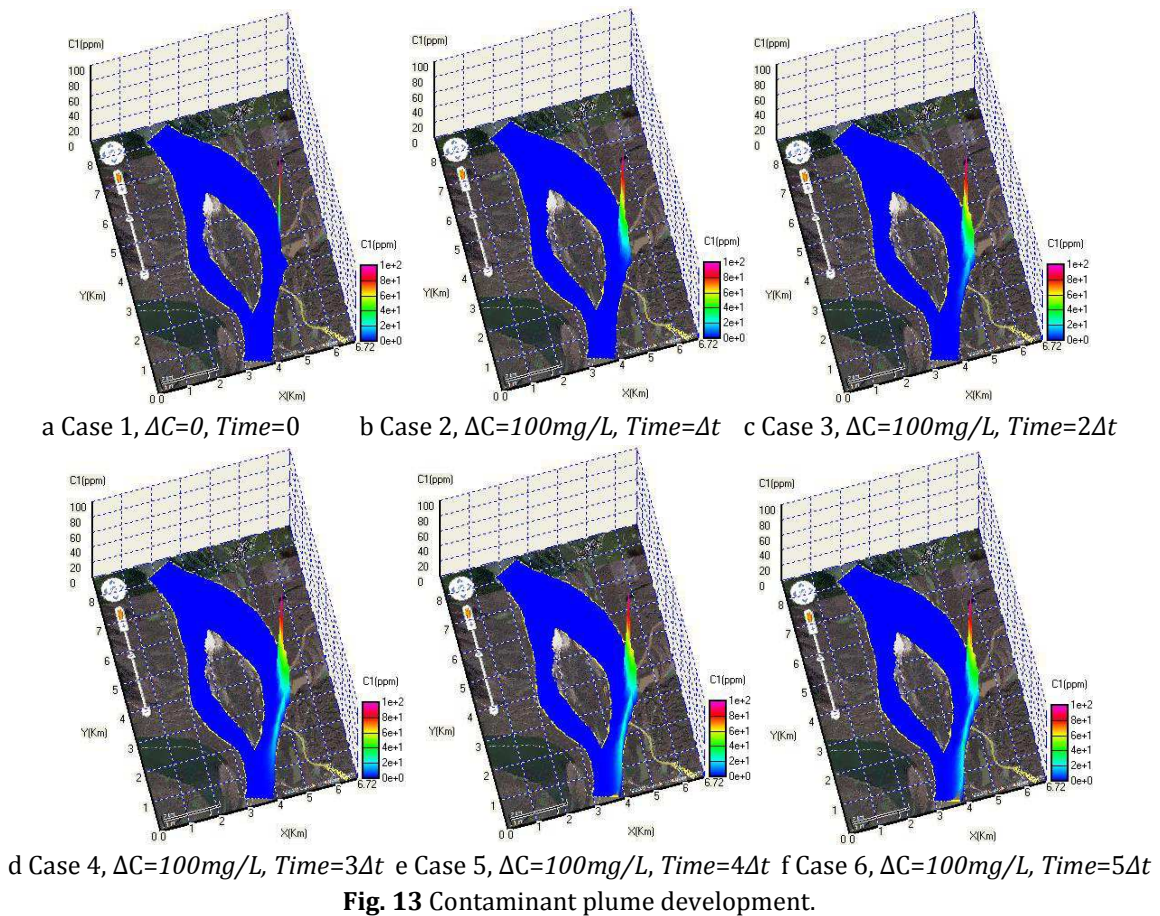


Fig. 12  $\tilde{\omega}$ ,  $\tilde{\epsilon}$  and  $\tilde{w}$  at a:  $i=32$  and  $j$  from 1 to 140; b:  $i$  from 1 to 34 and  $j=40$ .

### 6 Contaminant Plume Development at the Beginning of Discharge

In order to well understand the development process of pollutant plume, a special simulation was performed by using  $\tilde{k} - \tilde{\omega}$  model for the case described as follows. Supposing the contaminant concentration of the tributary firstly to equal zero, and then, the value of concentration instantaneously reaches  $100\text{mg/L}$  at  $Time=0$ , while the flow-rates, either of main stream or of tributary, keep constant. Figures 13a-f illustrate the plume development and variation in the lower reach of tributary outlet section, where Figure 13a presents the situation of clean water

confluence; Figures 13b-f display the process of contaminant impouring and plume development, with an equal time difference  $\Delta t$  each other.



## 7 Discussions and Conclusions

Two-equation models are one of the most common types of turbulence closure models. The so-called 'standard' two-equation turbulence models, adopted widely in industry, cannot be directly used in depth-averaged modeling. Till now, the vast majority of quasi 3D numerical tools in the world, using two-equation turbulence model to solve complete and non-simplified hydrodynamic fundamental governing equations, just can provide only one depth-averaged turbulence model ( $\tilde{k} - \tilde{\epsilon}$ ) for users, which appears already beyond 30 years. However, the advanced commercial CFD (*Computational Fluid Dynamics*) software for 'standard' 2D and 3D modeling already can provide several, even up to dozens of two-equation closure turbulence models, because there is non-existent a 'universal' turbulence closure model in the theory of turbulence modeling. Moreover, two-equation turbulence models are also very much still an active area of research and new refined two-equation models are still being developed. This situation should be changed as soon as possible.

At present, the  $k-\omega$  model, just like the  $k-\epsilon$  model, has become industry standard model and is commonly used for most types of engineering problems. Therefore, the establishment of depth-averaged  $\tilde{k} - \tilde{\omega}$  turbulence model and the numerical investigation and comparison with existing depth-averaged turbulence models, presented in this paper, are significant.

Two levels' grids, one coarse mesh and one fine mesh, were used in current simulation. The simulation on these two grids can satisfy the computational demand. If it is necessary, by setting the number of grid levels at three in the developed software, for example, the computations not only on coarse and fine grids but also on finest grid can be realized. The selection of the number of grid levels depends on the solved problems and modeler's requirements.

The solved depth-averaged concentration variable in current computation is the contaminant concentration difference between confluent tributary and main stream (100mg/L). However, other indexes of discharged contaminant, such as COD and BOD, also can be considered as the solved variable. The developed software possesses the ability to simultaneously solve two concentration components in one calculation, which are produced by industrial and domestic discharges.

Figure 7 demonstrates that the distributions of turbulent variable  $\tilde{k}$ , calculated by three turbulence models, vary strongly in the computational domain, but quite similar to one another. However, the characteristics of the distributions of  $\tilde{\omega}$ ,  $\tilde{\epsilon}$  and  $\tilde{w}$ , shown in Figures 8a, 8b and 8c, respectively, are different from one another, though they also vary sharply. The calculated effective viscosity  $\tilde{\mu}_{eff}$ , presented in Figures 9a, 9b and 9c, also varies strongly. In fact, the eddy viscosity changes from point to point in the computational domain, especially in the areas near the riversides and boundaries of island. To solve the problems of contaminant transport caused by side discharge, for example, the plume usually develops along a region near riverside (see Figure 6d and Figure 13), where  $\tilde{\mu}_t$  (or  $\tilde{\mu}_{eff}$ ) actually varies much strongly (see Figure 9). This means that  $\tilde{\mu}_t$  should be precisely calculated using suitable higher-order turbulence closure models with higher precision, and cannot be simply considered as an adjustable constant.

Figure 11 shows that the concentration profiles along the east riverbank, either calculated by  $\tilde{k} - \tilde{\omega}$  and  $\tilde{k} - \tilde{\epsilon}$  closures, or calculated by  $\tilde{k} - \tilde{w}$  closure, only have a quite small difference from one another. This means that three utilized depth-averaged two-equation turbulence models almost have the same ability to simulate plume distributions along riverbank. This conclusion also coincides with the result of author's previous research that the depth-averaged two-equation turbulence models are suitable for modeling strong mixing turbulence (Yu and Righetto, 2001). However, the abilities and behaviors of different depth-averaged two-equation turbulence models for rather weak mixing, also often encountered in engineering, should be further investigated.

Except for the different definitions of transported variables:  $\tilde{\epsilon}$ ,  $\tilde{w}$  and  $\tilde{\omega}$ , the order of magnitude of  $\tilde{\epsilon}$  is smaller than the order of magnitude of  $\tilde{w}$ , and much smaller than the order of magnitude of  $\tilde{\omega}$ . It should be noticed that three transported variables:  $\tilde{\epsilon}$ ,  $\tilde{w}$  and  $\tilde{\omega}$  all appear in the denominators of Eqs. (9), (14) and (2), which were used to calculate turbulent eddy viscosity  $\tilde{\mu}_t$ . For numerical simulation, the occurrence of numerical error is unavoidable, especially in the region near irregular boundary. It is clear that a small numerical error, caused by solving  $\tilde{\epsilon}$ -eq., for example, will bring on larger error for calculating eddy viscosity than the same error caused by solving other two equations (*i.e.*,  $\tilde{w}$ -eq. and  $\tilde{\omega}$ -eq.). Without doubt, the elevation of the order of magnitude of used second turbulent variable, reflecting the advance of two-equation turbulence closure models, provides a possibility for users to improve their computational precision. The insufficiency of traditional depth-averaged  $\tilde{k} - \tilde{\epsilon}$  turbulence model may be avoided by adopting other turbulence models that have appeared recently, such as the  $\tilde{k} - \tilde{\omega}$  model.

The developed *Graphical User Interface* of **Q3drm1.0** software can be used in various Windows-based microcomputers. The pre- and post-processors of this developed numerical tool, supported by a powerful self-contained map support tool together with a detailed help system, can help the user to easily compute the flows and contaminant transport behaviors in various natural waters, closed by using three different depth-averaged two-equation turbulence models, and to draw and analyze a wide variety of 2D and 3D engineering graphics for computed results.

### Acknowledgement

The partial support of FAPESP through the Process No. PIPE 2006/56475-3 is gratefully acknowledged.

## References

1. Cea L, Pena L, Puertas J, Vázquez-Cendón ME, Peña E (2007). Application of several depth-averaged turbulence models to simulate flow in vertical slot fishways. *J. Hydraulic Engineering*. 133(2): 160-172.
2. Chapmam RS, Kuo CY (1982). A Numerical Simulation of Two-Dimensional Separated Flow in a Symmetric Open-Channel Expansion Using the Depth-Integrated Two Equation ( $k$ - $\epsilon$ ) Turbulence Closure Model. Dept. of Civ. Engrg., Rep. 8202, Virginia Polytechnic Inst. and State Univ., Blacksburg, VA.
3. Choi M, Takashi H (2000). A numerical simulation of lake currents and characteristics of salinity changes in the freshening process. *J. Japan Society of Hydrology and Water Resources*, 13(6): 439-452.
4. Ferziger JH, Peric M (2002). *Computational Methods for Fluid Dynamics*, 3rd Edition. Berlin, Springer.
5. Hua ZL, Xing LH, Gu L (2008). Application of a modified quick scheme to depth-averaged  $k$ - $\epsilon$  turbulence model based on unstructured grids. *J. Hydrodynamics Ser. B(4)*, 514-523.
6. Ilegbusi JO, Spalding DB (1982). Application of a New Version of the  $k$ - $w$  Model of Turbulence to a Boundary Layer with Mass Transfer. CFD/82/15. London, Imperial College.
7. Johnson HK, Karambas TV, Avgeris I, Zanuttigh B, Gonzalez-Marco D, Caceres I (2005). Modelling of waves and currents around submerged breakwaters. *Coastal Engineering*. 52(10): 949-969.
8. Kimura I, Uijtewaal WSJ, Hosoda T, Ali MS (2009). URANS computations of shallow grid turbulence. *J. Hydraulic Engineering*. 135(2): 118-131.
9. Kirkgoz MS, Akoz MS, Oner AA (2009). Numerical modeling of flow over a chute spillway. *J. Hydraulic Research*. 47(6): 790-797.
10. Kwan S (2009). A Two Dimensional Hydrodynamic River Morphology and Gravel Transport Model. Master (MAsc) Degree Thesis, University of British Columbia.
11. Lee JT, Chan HC, Huang CK, Wang YM, Huang WC (2011). A depth-averaged two-dimensional model for flow around permeable pile groins. *International J. the Physical Sciences*. 6(6): 1379-1387.
12. Lunis M, Mamchuk VI, Movchan VT, Romanyuk LA, Shkvar EA (2004). Algebraic models of turbulent viscosity and heat transfer in analysis of near-wall turbulent flows. *International J. Fluid Mechanics Research*. 31(3): 60-74.
13. McGuiirk JJ, Rodi W (1977). A Depth-Averaged Mathematical Model for Side Discharges into Open Channel Flow. SFB 80/T/88. Universität Karlsruhe.
14. Mei Z, Roberts AJ, Li ZQ (2002). Modeling the Dynamics of Turbulent Floods. *SIAM J. Applied Mathematics*. 63(2): 423-458.
15. Riasi A, Nourbakhsh A, Raisee M (2009). Unsteady turbulent pipe flow due to water hammer using  $k$ - $\omega$  turbulence model. *J. of Hydraulic research*. 47(4): 429-437.
16. Rodi W, Pavlovic RN, Srivatsa SK (1980). Prediction of flow pollutant spreading in rivers. In: *Transport Models for Inland and Coastal Waters: Proceedings of the Symposium on Predictive Ability*. Berkeley: University of California Academic Press, pp 63-111.
17. Saffman PG (1970). A model for inhomogeneous turbulent flow. In: *Proc. Roy. Soc. London*. A317, pp 417-433.
18. Vasquez JA (2005). Two Dimensional Finite Element River Morphology Model. Ph. D. Dissertation, University of British Columbia.
19. Viparelli E, Sequeiros OE, Cantelli A, Wilcock PR, Parker G (2010). River morphodynamics with creation/consumption of grain size stratigraphy 2: numerical model. *Journal of Hydraulic Research*. 48(6): 727-741 Wilcox DC (1998). *Turbulence Modeling for CFD*. La Canada, DCW Industries, Inc.
20. Yu LR, Zhang SN (1989). A new depth-averaged two-equation ( $\tilde{k} - \tilde{w}$ ) turbulent closure model. *J. Hydrodynamics Series*. B(1): 47-54.
21. Yu LR, Righetto AM (2001). Depth-averaged turbulence  $\tilde{k} - \tilde{w}$  model and applications. *Advances in Engineering Software*. 32(5): 375-394.
22. Yu LR (2013). *Quasi 3D Modeling Flow and Contaminant Transport in Shallow Waters* (ISBN: 978-3-659-33894-6). LAP LAMBERT Academic Publishing, Germany.